

New approach for multi-material design: Combination of laser beam and electromagnetic melt pool displacement by induced Lorentz forces


Cite as: J. Laser Appl. 35, 012001 (2023); <https://doi.org/10.2351/7.0000763>

Submitted: 21 June 2022 • Accepted: 09 November 2022 • Published Online: 01 December 2022

 Jennifer Heßmann and  Kai Hilgenberg

COLLECTIONS

Note: Paper published as part of the special topic on Proceedings of the International Congress of Applications of Lasers & Electro-Optics 2022.

 This paper was selected as Featured



View Online



Export Citation



CrossMark



ICALEO
40th INTERNATIONAL CONGRESS ON
APPLICATIONS OF LASERS & ELECTRO-OPTICS

SPECIAL ISSUE: International Congress on
Applications of Lasers & Electro-Optics (ICALEO® 2021)

Read Now!

New approach for multi-material design: Combination of laser beam and electromagnetic melt pool displacement by induced Lorentz forces

Cite as: J. Laser Appl. **35**, 012001 (2023); doi: [10.2351/7.0000763](https://doi.org/10.2351/7.0000763)

Submitted: 21 June 2022 · Accepted: 9 November 2022 ·

Published Online: 1 December 2022



View Online



Export Citation



CrossMark

Jennifer Heßmann^{a)}  and Kai Hilgenberg 

AFFILIATIONS

BAM Bundesanstalt für Materialforschung und-prüfung, Unter den Eichen 87, 12205 Berlin, Germany

Note: Paper published as part of the special topic on Proceedings of the International Congress of Applications of Lasers & Electro-Optics 2022.

^{a)}Electronic mail: jennifer.hessmann@bam.de

ABSTRACT

Multimaterial structures are a promising solution to reduce vehicle weight and save fuel or electric energy in automotive design. However, thermal joining of steel and aluminum alloys is a challenge to overcome due to different material properties and the formation of brittle intermetallic phases. In this study, a new joining approach for producing overlap line-shaped joints is presented. The lower joining partner (EN AW 5754) is melted by a laser beam, and this melt is displaced into a line-shaped cavity of the upper joining partner (1.0330) by induced Lorentz forces. The melt solidifies in the cavity to a material and form-fitting joint. This approach needs no auxiliary joining elements or filler materials. Previous investigation to produce spot-shaped joints by using this approach showed that quality and reproducibility were limited by known melt pool dynamics of aluminum alloys (keyhole collapses). For line-shaped joints, the melt displacement can take place behind the keyhole. This allows the displacement process to be spatially uncoupled from the influence of keyhole collapses. The study shows that this improved the process stability and the quality of the joint. The created line-shaped joints were microstructurally characterized by transversal sections. Intermetallic phases were identified by electron backscatter diffraction and EDX analysis. The detected intermetallic phases consist of a 5–6 μm compact phase seam of $\text{Al}_{5,6}\text{Fe}_2$ and a needle-shaped phase of $\text{Al}_{13}\text{Fe}_4$. Tensile shear tests were carried out to quantify the load capacity. It was possible to create a joint with a load capacity of about 2 kN.

Key words: laser beam welding, electromagnetic forces, Lorentz forces, melt pool displacement, dissimilar materials, steel and aluminum

© 2022 Author(s). All article content, except where otherwise noted, is licensed under a Creative Commons Attribution (CC BY) license (<http://creativecommons.org/licenses/by/4.0/>). <https://doi.org/10.2351/7.0000763>

INTRODUCTION

The trend toward lightweight vehicles is leading to a mix of materials to produce function and weight-optimized car bodies.¹ This so-called multimaterial design is a promising solution to reduce the weight of the vehicle, to protect the environment, and to extend the range of electric cars.^{2,3} To realize the multimaterial design, the joining of dissimilar materials is necessary. For the automotive industry, the material combination of steel and aluminum alloy is of interest.⁴ However, thermal joining of steel and aluminum is difficult.²

The different material properties, e.g., melting temperatures and thermal expansion coefficients, complicate the joining process. In addition, due to the insolubility between Fe and Al, intermetallic phases form, which reduce the quality and the load capacity of the joint.⁵ Several studies have investigated the metallurgical reaction between solid steel and liquid aluminum alloys. Mainly, a two-phase reaction layer consisting of a needle-shaped Al_3Fe (also known as $\text{Al}_{13}\text{Fe}_4$ ⁶) and a compact phase seam of Al_5Fe_2 is formed.^{7,8} These phase compositions are mainly formed since they have the lowest free

enthalpies of all Fe-Al phases.⁹ To obtain sound joints, the thickness of the intermetallic reaction layer should not exceed the critical value of $10\ \mu\text{m}$.¹⁰ These two intermetallic phase compositions are very brittle with hardness values of 820–1100 HV.¹¹ The formation of the intermetallic phases is a diffusion-controlled process and cannot be prevented. It is only possible to control the thickness of these phases below the critical value of $10\ \mu\text{m}$. For this, the maximum temperatures and the interaction time within the joining process should be limited as much as possible.^{9,12} Solid-phase welding and joining processes with a low heat input such as welding-brazing are ideal for this task.¹³ Laser beam welding-brazing has been studied for joining steel and aluminum alloy. Wang *et al.* analyzed the microstructure of a dissimilar overlap joint between 1 mm galvanized DP590 steel and 1 mm 6061 aluminum alloy by experiments and numerical simulation. They show that with increasing line energy density the thickness of the intermetallic phases increases, and the presence of these phases affects the tensile strength of the welded joint. They detected the phases Al_3Fe_2 and $\text{Al}_{13}\text{Fe}_4$ with a maximal thickness of $20\ \mu\text{m}$ at 162 J/mm. They achieved the best tensile strengths at 162 J/mm with 1.7 kN.⁸ Huang *et al.* investigated the process window and its influence on the interfacial microstructure and mechanical properties of laser welded-brazed joints between 1.9 mm 22MnB5 steel and 1.5 mm 6061 aluminum alloy. In addition, they used a Zn-Al₁₅ filler material. They show that the additional Zn creates new compositions of intermetallic phases. They detected $\text{Fe}_2(\text{Al}, \text{Zn})_3$ and FeZn_{10} , which are more ductile than the conventional intermetallic phases produced without a Zn containing filler material. The thickness of the intermetallic phases was between 0.47 and $11.13\ \mu\text{m}$. They reached a max. tensile force of 2793 N.¹⁴ In the study of Windmann *et al.*, 1.5 mm sheets of aluminum-coated high-strength 22MnB5 steel and 6016 aluminum were joined by laser beam welding-brazing. They used AlSi_3Mn as the filler metal and analyzed the resulting microstructure at different welding energies. They confirm that the thickness of the intermetallic phases increases at higher heat input. The growth of the intermetallic phases is influenced by the Si-containing filler material. They observed the formation of $\text{Al}_8\text{Fe}_2\text{Si}$ and $\text{Al}_{13}\text{Fe}_4$ phases. The thickness ranged around 2– $15\ \mu\text{m}$ and resulted in maximum tensile strengths of 1900–2800 N with a wetting length of about 2.4 mm at a laser power of 3.3 kW.¹⁵ Yang *et al.* also investigated the formation of intermetallic phases and their influence on the load capacity of a lap joint of 1 mm galvanized DP980 steel and 1.5 mm 5754 aluminum alloy. They used Zn_{22}Al as the filler material. By forming a ductile reaction layer consisting of FeZn_{10} +amorphous al-rich phase and $\text{Fe}_2\text{Al}_{5-x}\text{Zn}_x$, the joint reaches a maximum tensile force of 1200 N, although the thickness of the intermetallic phases is between 20 and $45\ \mu\text{m}$. They observed two failure modes: the failure at the reaction layer and the failure within the fusion zone. The authors explain the failure of the fusion zone not by the thickness of the intermetallic phases but rather by the geometry of the fusion zone.¹⁶ All these investigations produced a load-bearing material-fit joint with or without a filler material. An additional form fit could increase the strength of the joints. To achieve a form fit, the filling of a conical cavity is necessary. To improve the lightweight balance and to save production costs, it is advantageous to use a joining process that does not require any filler material or auxiliary joining elements. Therefore, a controlled movement of the melt is needed. Liquid metals are electrically conductive media and can be

influenced by magnetic fields during a welding process. The use of the electromagnetically melt pool influence could already be demonstrated for different applications. For example, when welding thick plates with filler wire, unsatisfactory mixing of the filler metal in the weld pool can occur. It results in a nonuniform element distribution in the weld seam. Üstündag *et al.* show that an oscillating magnetic field improves the element distribution over the whole thickness of a 20 mm thick laser beam welded S355J2 steel plate.¹⁷ Another example is the melt pool support to prevent drop out when welding thick sheets. Fritzsche *et al.* demonstrate this for a 20 mm thick ferromagnetic duplex and mild steel sheet.¹⁸ In the described examples, the magnetic field influences the melt pool flows. This offers a basis for a new approach to join dissimilar materials.

NEW APPROACH FOR JOINING DISSIMILAR MATERIALS

The new approach is schematically shown in Fig. 1. This joining method combines melt pool generation by a laser beam and a controlled melt pool displacement by an AC magnetic system. The joining partners are placed in an overlap configuration, whereby the upper joining partner must have a significant higher melting temperature and a conical cavity. The laser beam melts the lower joining partner through this cavity (Fig. 1 left side). The AC magnetic system is placed below the overlap configuration and induces upward directed electromagnetic forces (Lorentz force F_L). This Lorentz force causes a movement of the melt, so that the cavity of the upper joining partner is filled (Fig. 1 right side). After the displacement process, the laser beam is turned off. The moved melt solidifies in a material- and form-fitting joint.

With this method, the formation of intermetallic phases can be reduced because only one joining partner was melted and wets the solid joining partner. This approach can be used for spot- and line-shaped joints and needs no filler materials or auxiliary joining elements. In the work of Heßmann *et al.*, more details of the displacement process can be read.¹⁹ They tested this new joining method to create spot-shaped joints between 2 mm 5754 aluminum alloy and 1 mm 1.0330 steel. They find out that an equilibrium is achieved between the downward and upward directed forces, which limits the height of the melt displacement. The forces are the hydrostatic pressure, the Laplace pressure, and the electromagnetic pressure. The formation of many spatters could be observed at high-speed camera recordings due to the known melt pool dynamic of an aluminum alloy during laser beam deep welding. As a result, a part of the molten material is lost, which sometimes leads to a cavity that is not completely filled. In some cases, cracks are visible in the transverse sections, which reduce the load-bearing capacity of the joints. They found a magnetic field power of about 300–2000 W to be sufficient for a displacement process. They also show that the displacement needs less time at higher electromagnetic forces compared to lower electromagnetic forces.¹⁹

This study tests the new approach for line-shaped joints. Based on the findings of the spot-shaped joints, in this case the process is spatially decoupled from the keyhole to optimize the displacement process. Thus, it is to be expected that the influence of the keyhole collapse can be reduced. The created linear joints were microstructurally and mechanically characterized.

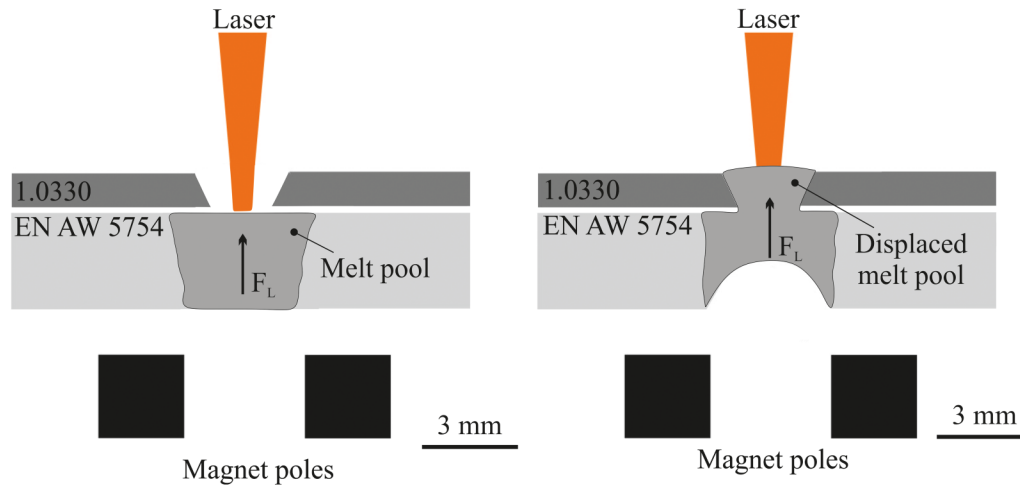


FIG. 1. Schematically illustration of the new joining approach for line-shaped joints, front view.

EXPERIMENTS

The experimental set up is shown in Fig. 2. A 3 mm aluminum alloy (EN AW 5754) and a 1 mm steel sheet (1.0330) were used and placed in an overlap configuration, whereby the aluminum sheet was below the steel sheet. The measured chemical compositions of the used materials are shown in Table I. To displace the generated melt pool, a self-constructed AC magnetic system was placed 2 mm below the overlap configuration. More details of the used AC magnetic system and the calibration procedure can be read in the work of Heßmann *et al.*¹⁹ and Fritzsche *et al.*¹⁸ To limit the range of the

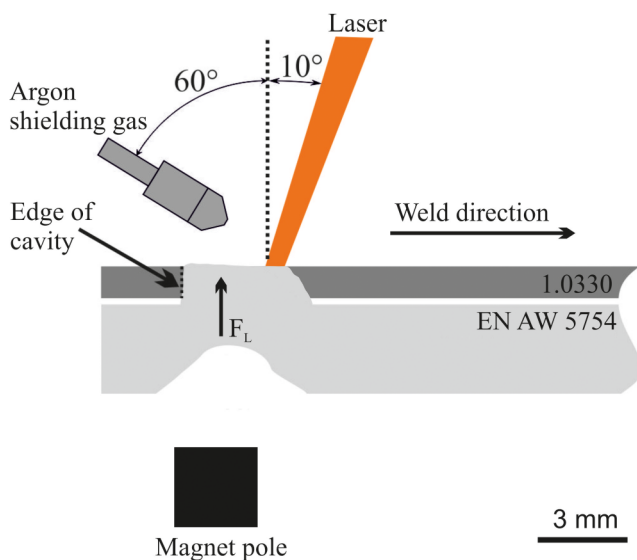


FIG. 2. Schematically illustration of the experimental set up, side view.

magnetic field to 4 mm, a frequency of 3750 Hz was used. This reduced the interactions with the ferromagnetic steel.

The cavity of the steel sheet was 30° beveled, 3 mm wide, and 100 mm long. This conical cavity is important to create an additional form fit to the material fit. If the cavity is not conical, it is not possible to produce a joint due to the different thermal expansion coefficients of the joining partners. The sheets were fixed in a clamping system to ensure the technical zero gap. An IPG YLR 20 000 fiber laser was used, and the optics was tilted by 10° against the weld direction. The position of focus was 10 mm above the upper sheet, and argon with a flow rate of 20 l/min was used as the shielding gas. The Argon gas nozzle was tilted by 60°. The laser spot was positioned on the outer edge of the magnetic pole shoes to spatially decouple the keyhole and the displacement process. Details of the laser system and the used process parameters are listed in Table II. The laser parameters were evaluated by

TABLE I. Chemical compositions of the used materials.

Element	Content in mass-%	
	EN AW 5754	1.0330
Si	0.08	—
Fe	0.30	Bal.
Cu	0.02	—
Mn	0.50	0.10
Mg	3.30	—
Cr	0.01	—
Zn	0.01	—
Ti	0.02	—
Al	Bal.	—
C	—	0.02
S	—	0.01
P	—	0.02

TABLE II. Details of the laser system and the AC magnetic system.

Typ of laser	IPG YLR 20 000
Maximum laser output	20 kW
Diameter of fiber	200 μm
Diameter of laser spot	937 μm
Position of focus	10 mm
Wavelength	1070 nm
Focal length	350 mm
Beam parameter product	11 mm \times mrad
Angle of laser optic	10°
Inert gas	Argon
Flow rate of inert gas	20 l/min
Angle of inert gas nozzle	60°
Laser power	3300 W
Weld speed	1.3 m/min
Magnetic field power	670 W
Frequency	3750 Hz

preliminary tests to ensure a stable reproducible melt pool. The magnetic field power of 670 W was selected based on the findings of Heßmann *et al.*¹⁹ The joining method was repeated twice. Three transversal sections of the created line joints were prepared to analyze the filling of the cavity (etching: 2% Nital and 2% NaOH). The grain size was also determined by the line intersection method. In addition, laser profile scans were carried out to evaluate the complete displacement height and quality of the line joints. A SEM LEO Electron Microscopy Inc. type 1530 VP was used to identify the intermetallic phases at the interface by electron backscatter diffraction (EBSD). Therefore, the specimen was tilted by 70°. The voltage of the electron beam was 20 kV, and the detector was tilted by 4°. The exposure time was 150 ms and the size of the analyte was 200 \times 150 pixel. In addition, energy dispersive x-ray spectroscopy (EDX) measurements were carried out to identify the intermetallic phases (IMC). Hardness profile test according to Vickers (HV 0.01) was done to analyze the development of hardness in the area of the displaced aluminum melt and the steel sheet. Tensile shear tests were carried out for the magnetic field of 670 W to quantify the load capacity of the line joints. These five additional

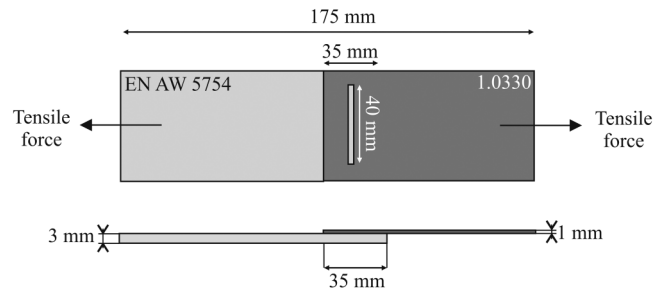


FIG. 3. Schematically illustration of the tensile shear test specimens top view and side view.

tensile specimens with a weld length of 40 mm and an overlap of 35 mm were produced and tested at a test speed of 1 mm/min. Before the tensile shear test, the specimens were x ray tested for internal cracks and pores in a nondestructive way (resolution, 25 μm). The local strains of the specimens were optically monitored by the GOM ARAMIS system and checked by an extensometer measurement. For this, the surface of the tensile shear specimens was sprayed with a black and white pattern. Figure 3 shows the top view and side view of an exemplary tensile shear specimen.

RESULTS AND DISCUSSION

Figure 4 shows the top and bottom sides of the created line-shaped joint by photographs and laser profile scans. The top side of the joint has a uniform filling of the cavity without spatters and edge overlaps of the displaced melt. The laser profile scan of the top side shows a height of the displaced melt pool of about 0.5 mm over the upper edge of the steel sheet. The bottom side of the displaced melt is wavy shaped. The bottom side shows also a uniform displacement of the aluminum melt in the laser profile scan.

An exemplary transverse section is shown in Fig. 5. A magnetic field power of 670W is sufficient for a complete filling of the cavity. In some cases, some pores can be observed in the cross sections around the bottom side of the steel sheet. The pores could be air injections coming from the gap between the steel and the

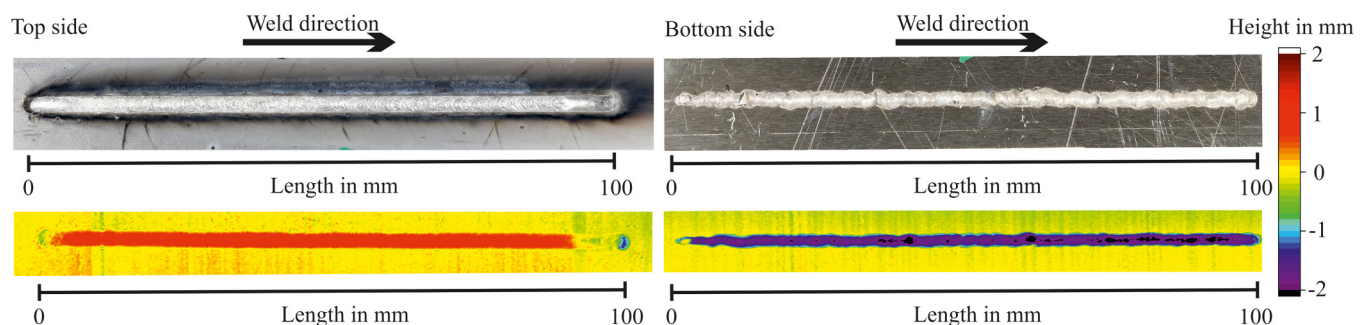


FIG. 4. Photographs and profile scans of the line joint top and bottom side.

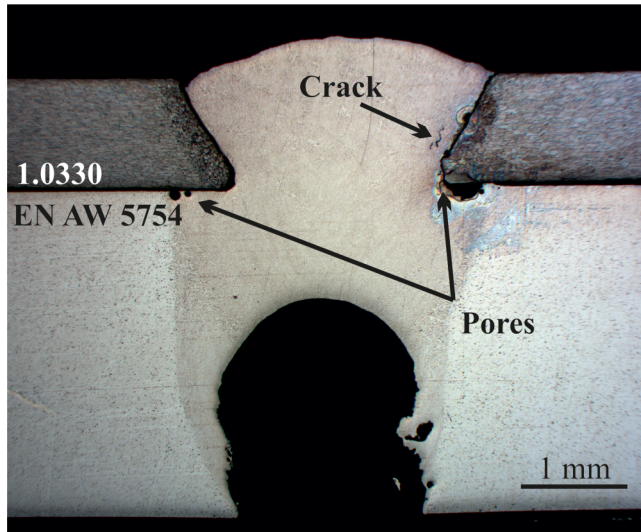


FIG. 5. Exemplary transverse section of the displaced melt.

aluminum sheet. The air bubbles could not escape during the joining process. Rarely, cracks have been found. These cracks are very rare and small. Thus, the cracks are acceptable.

Compared to the spot joints investigated by Hefßmann *et al.*,¹⁹ the joining process for line joints is significantly more stable and effective. It was possible to achieve significantly higher displacements with a low magnetic field power of 670 W compared to the spot joints. The melt was displaced minimally above the upper edge of the steel sheet. The influence of the melt pool dynamics was successfully reduced by spatial decoupling. The intermetallic phases were identified using EBSD- and EDX-analyses and are shown in Fig. 6. A compact phase seam at the interface toward the steel side has formed. This is followed by an acicular phase toward

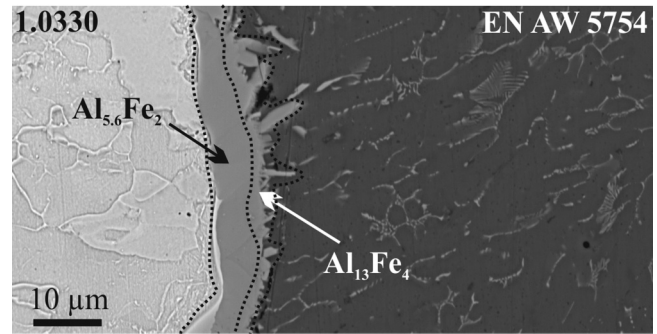


FIG. 6. The intermetallic phases at the interface between solid steel and displaced liquid aluminum alloy.

the aluminum side. The compact seam could be identified as the phase composition $Al_{5,6}Fe_2$ with about 73 at. % Al and 27 at. % Fe. The acicular phase consists of $Al_{13}Fe_4$ with about 83 at. % Al and 17 at. % Fe. The thickness of the compact phase seam is in average $5.7 \pm 1.9 \mu m$. The needle-shaped phases have an average length of $1.3 \pm 0.6 \mu m$. Locally, the formation of significantly different dimensions of IMC was observed. Overall, the formed intermetallic phases are below the critical value of $10 \mu m$. In agreement with the findings from Refs. 6–8, a two-phase reaction layer was also formed in this process. Normally, the Al_5Fe_2 phase is detected. It is known from the work of Szczepaniak *et al.* that high cooling rates exist in the case of laser beam welding. Due to these high cooling rates, intermetallic phase compositions can form different from the equilibrium state.²⁰ Thus, in our study, a non-equilibrium phase of Al_5Fe_2 has been formed.

The results of the hardness profile measurement are shown in Fig. 7. The hardness of the steel is about 150 HV 0.01 and increases to about 200 HV 0.01 in the heat-affected zone (HAZ). The measured chemical composition of the used steel sheet of Table I shows that the steel contains a very low carbon content of 0.02 mass-%.

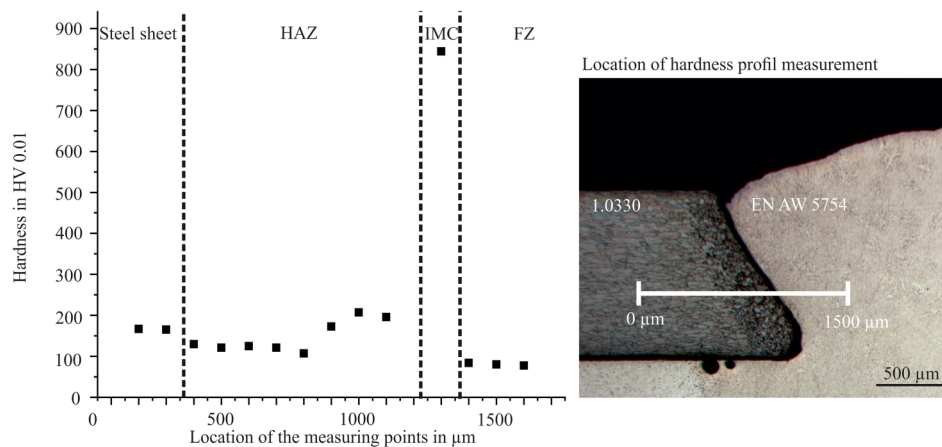


FIG. 7. Hardness profile of the created line joint.

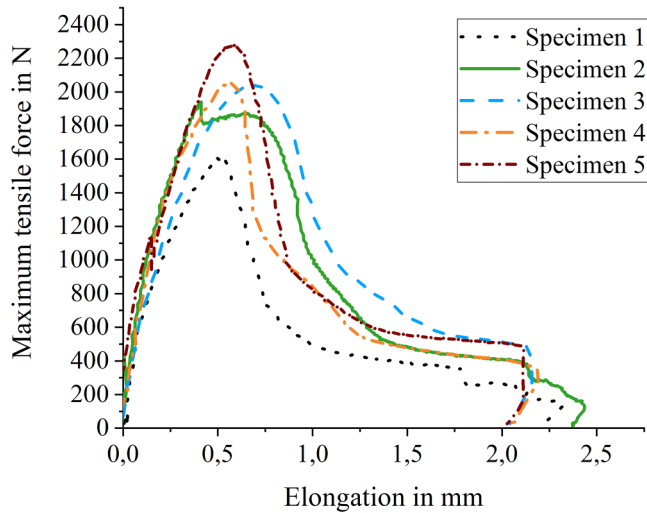


FIG. 8. The force-elongation curves of the five tensile shear tests.

So, martensite formation is not possible. The steel sheet is cold rolled. Thus, the steel already contains a high dislocation density. Furthermore, additional deformations were added by the production of the long conical cavity. During the displacement process, temperatures of up to about 1300 °C occur in the steel sheet.¹⁹ Thus, a recrystallization process is possible. Grain size analyses using line intersection methods have shown that the average grain size is reduced from about 17 μm to about 9 μm . The recrystallization has resulted in a very fine microstructure in the HAZ compared to the base metal, thereby increasing its hardness by grain boundary strengthening. The base metal aluminum has a hardness of about 60 HV 0.01. The fusion zone (FZ) shows hardness values of about 85 HV 0.01. In the SEM images, only at the interface, intermetallic phases (IMC) were found but not in the middle of the displaced aluminum melt. Thus, the increase in hardness can also be explained by a fine grain resulting from the solidification process. A typical dendritic structure with a dendrite size of about

4–6 μm has formed. The base material has an average grain size of about 12 μm . The highest hardness value of about 840 HV 0.01 was achieved directly at the interface due to the formed intermetallic phases. It agrees with the reported values of the phase composition of Al_5Fe_2 and $\text{Al}_{13}\text{Fe}_4$.¹¹

The force-elongation curves of the tensile shear tests are shown in Fig. 8. In the previously performed x-ray tests, no cracks or pores could be detected. The different curve profiles are caused by the locally differently formed thicknesses of the IMC. The dimension of the IMC has a significant influence on crack initiation and propagation. In the work of Windmann *et al.*, also a significant range of thickness of the IMC (2–15 μm) could be observed and resulted in a significant variation of the maximum tensile strengths of 1900–2800 N.¹⁵

In our study, the line joints can bear a maximum force of 2300 N with an elongation of 2 mm. All the samples failed in the same way: The displaced aluminum melt did not fail or shear off during the entire tensile shear test. Also, the steel sheet did not break. At first, the material fit failed. The formed intermetallic phases at the interface are the weakest region in the joint due to their brittle properties. In addition, the intermetallic phases have a low ductility as well as a high crack sensitivity. The results of the hardness measurements show that the highest hardness in the joint is achieved in the IMC. The two different IMCs were identified as Al-rich phases.

These are known to be very brittle and sensitive for cracking. As a result, the material fit fails first under the maximum tensile force. The form fit still holds the sheets together. During tensile loading, the 40 mm long cavity becomes wider due to the elongation of the steel sheet and the end of the steel sheet bends upward. When the maximum elongation is reached, the form fit finally also breaks. The described steps of the failure of tensile shear specimen can be exemplarily seen in Fig. 9.

The measured tensile shear values correspond to the values reported by Wang *et al.* for welding-brazing without the use of a filler metal.⁸ However, the authors did not specify the tested joint length. The results of this work cannot be compared exactly with the values of the literature because in other studies filler materials or other base materials were used. The tested specimens in this research without the use of a filler material show that it is possible to produce a similarly strong joint only by a controlled melt pool displacement.

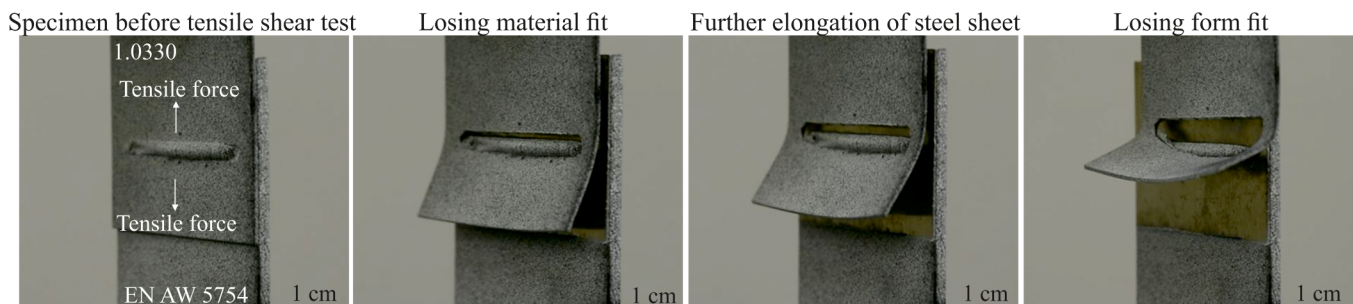


FIG. 9. Exemplary failure steps of tensile shear specimen.

SUMMARY

In this study, a new joining approach for line-shaped joints was tested. The spatial decoupling between the displacement process and the keyhole dynamic improves the melt pool displacement process. The microstructure and the mechanical properties of the created line joints were analyzed. The results can be summarized as follows:

- With a magnetic field power of 670 W, a uniform aluminum melt displacement is possible so that the cavity is filled completely.
- Compared to previous studies on the creation of spot joints, the displacement process is more stable and effective. Higher displacement heights are possible.
- A two-phase reaction layer was detected, and it consists of a 5.7 μm compact phase seam on the steel side and a following needle-shaped structure toward the aluminum side. The needles are on average 1.3 μm long and consist of the $\text{Al}_{13}\text{Fe}_4$ phase. The compact phase seam was detected as $\text{Al}_{5,6}\text{Fe}_2$. The thickness of the intermetallic phases is below the critical value of 10 μm .
- The hardness values compared to the base metals increase in the HAZ and FZ. In the HAZ, a very fine grain structure with an average grain size of 9 μm is formed. The FZ consists of a cast structure with a size of dendrites of about 4–6 μm .
- Tensile shear tests show a maximum load capacity of 2300 N. The first failure starts in the material fit due to the brittle material properties of the intermetallic phases, where cracks can easily form and grow. Due to the elongation of the steel sheet, the cavity widens, so that finally the form fit also fails.

AUTHOR DECLARATIONS

Conflict of Interest

The authors have no conflicts to disclose.

Author Contributions

Jennifer Heßmann: Investigation (equal); Validation (equal); Visualization (equal); Writing – original draft (equal); Writing – review & editing (equal). **Kai Hilgenberg:** Writing – review & editing (equal).

REFERENCES

- ¹P. K. Mallik, *Materials, Design and Manufacturing for Lightweight Vehicles*, 2nd ed. (Elsevier Ltd., Joining for Lightweight Vehicles, Woodhead Publishing in Materials, Duxford, UK, 2021), pp. 321–369.
- ²Md. A. Karim and Y. D. Park, “A review on welding of dissimilar metals in car body manufacturing,” *J. Weld. Join.* **38**, 8–23 (2020).
- ³A. Kleine, M. Rosefort, and H. Koch, “Light metals, springer, lightweight construction for electric mobility using aluminium,” in *The Minerals, Metals & Materials Society*, edited by J. Grandfield (Springer, Cham, Switzerland, 2014), pp. 331–335.

- ⁴G. Meschut, O. Hahn, V. Janzen, and T. Olfemann, “Innovative joining technologies for multi-material structures,” *Weld. World* **58**, 65–75 (2014).
- ⁵G. Yu, S. Chen, S. Li, J. Huang, J. Yang, Z. Zhao, W. Huang, and S. Chen, “Microstructures and mechanical property of 5052 aluminum alloy/Q235 steel butt joint achieved by laser beam joining with Sn-Zn filler wire,” *Opt. Laser Technol.* **139**, 1–10 (2021).
- ⁶K. J. Lee and S. Kumai, “Characterization of intermetallic compound layer formed at the weld interface of the defocused laser welded low carbon steel/6111 aluminum alloy lap joint,” *Mater. Trans.* **47**, 1178–1185 (2006).
- ⁷H. Aghajani Derazkola and F. Khodabakhshi, “Intermetallic compounds (IMCs) formation during dissimilar friction-stir welding of AA5005 aluminum alloy to St-52 steel: Numerical modeling and experimental study,” *Int. J. Adv. Manuf. Technol.* **100**, 2401–2422 (2019).
- ⁸C. Wang, L. Cui, G. Mi, P. Jiang, X. Shao, and Y. Rong, “The influence of heat input on microstructure and mechanical properties for dissimilar welding of galvanized steel to 6061 aluminum alloy in a zero-gap lap joint configuration,” *J. Alloys Compd.* **726**, 556–566 (2017).
- ⁹G. Filliard, M. El Mansori, M. De Metz-Nobalt, C. Bremont, A. Reullier, and L. Tirado, “Influence of process parameters on thermal cycle and intermetallic compounds formation in high speed laser weld-brazing of aluminium-steel angle joints,” *Proc. Manuf.* **26**, 690–699 (2018).
- ¹⁰G. Filliard, M. El Mansori, L. Tirado, S. Mezghani, C. Bremont, and M. De Metz-Nobalt, “Industrial fluxless laser weld-brazing process of steel to aluminium athigh brazing speed,” *J. Manuf. Process.* **25**, 104–115 (2017).
- ¹¹R. Indhu, S. Soundarapandian, and L. Vijayaraghavan, “Yb:YAG laser welding of dual phase steel to aluminium alloy,” *J. Mater. Process. Technol.* **262**, 411–421 (2018).
- ¹²K. Szallies, M. Zwicker, and J. P. Bergmann in *Advanced Joining Processes, Advanced Structured Materials, Single-Sided Resistance Spot Welding of Steel-Aluminum Dissimilar Joints—Mechanical Characterization and Interface Formation*, edited by L. F. M. da Silva, P. A. F. Martins, and M. S. El-Zein (Springer Nature, Singapore, 2020), pp. 79–90.
- ¹³M. Pouranvari and M. Abbasi, “Dissimilar gas tungsten arc weld-brazing of Al/steel using Al-Si filler metal: Microstructure and strengthening mechanisms,” *J. Alloys Compd.* **749**, 121–127 (2018).
- ¹⁴R. Huang, C. Tan, Y. Sun, X. Gong, L. Wu, B. Chen, H. Zhao, and X. Song, “Influence of processing window on laser welding-brazing of Al to press-hardened 22MnB5 steel,” *Opt. Laser Technol.* **133**, 1–11 (2021).
- ¹⁵M. Windmann, A. Röttger, H. Kügler, W. Theisen, and F. Vollersten, “Laser beam welding of aluminum to Al-base coated high-strength steel 22MnB5,” *J. Mater. Process. Technol.* **217**, 1–25 (2014).
- ¹⁶J. Yang, Z. S. Yu, Y. L. Li, H. Zhang, W. Guo, P. Peng, and Y. N. Zhou, “Formation and toughening mechanisms of dispersions in interfacial intermetallics of dissimilar laser Al/steel joints,” *J. Mater. Eng. Perform.* **27**, 4107–4114 (2018).
- ¹⁷Ö. Üstündag, V. Avilov, A. Gumenyuk, and M. Rethmeier, “Improvement of filler wire dilution using external oscillating magnetic field at full penetration hybrid laser-arc welding of thick materials,” *Metals* **9**, 594 (2019).
- ¹⁸A. Fritzsche, V. Avilov, A. Gumenyuk, K. Hilgenberg, and M. Rethmeier, “High power laser beam welding of thick-walled ferromagnetic steels with electromagnetic weld pool support,” in *9th International Conference on Photonic Technologies-Lane*, September 19–22, Fürth, Germany (Elsevier B.V., 2016), pp. 362–372.
- ¹⁹J. Heßmann, M. Bachmann, and K. Hilgenberg, “Numerical and experimental investigation of controlled weld pool displacement by electromagnetic forces for joining dissimilar materials,” *Metals* **10**, 1–18 (2019).
- ²⁰A. Szczepaniak, J. Fan, A. Kostka, and D. Raabe, “On the correlation between thermal cycle and formation of intermetallic phases at the interface of laser-welded aluminum-steel overlap joints,” *Adv. Eng. Mater.* **14**, 464–472 (2012).